AIAA 2004-2805

Investigation of Volumetric Sources in Airframe Noise Simulations

Jay H. Casper*, David P. Lockard†, Mehdi R. Khorrami‡, and Craig L. Streett§
NASA Langley Research Center, Hampton, VA, 23681

Hybrid methods for the prediction of airframe noise involve a simulation of the near field flow that is used as input to an acoustic propagation formula. The acoustic formulations discussed herein are those based on the Ffowcs Williams and Hawkings equation. Some questions have arisen in the published literature in regard to an apparently significant dependence of radiated noise predictions on the location of the integration surface used in the solution of the Ffowcs Williams and Hawkings equation. These differences in radiated noise levels are most pronounced between solid-body surface integrals and off-body, permeable surface integrals. Such differences suggest that either a non-negligible volumetric source is contributing to the total radiation or the input flow simulation is suspect. The focus of the current work is the issue of internal consistency of the flow calculations that are currently used as input to airframe noise predictions. The case study for this research is a computer simulation for a three-element, high-lift wing profile during landing conditions. The noise radiated from this flow is predicted by a two-dimensional, frequency-domain formulation of the Ffowcs Williams and Hawkings equation. Radiated sound from volumetric sources is assessed by comparison of a permeable surface integration with the sum of a solid-body surface integral and a volume integral. The separate noise predictions are found in good agreement.

Nomenclature

c_0	=	ambient sound speed	t	=	time
f	=	dimensionless frequency	U_i	=	uniform, rectilinear surface velocity
$f(\vec{x},t)$	=	geometric surface function	u_i	=	local fluid velocity components
$G(x,y)$	=	Green's function	v_i	=	surface velocity components
$H(\cdot)$	=	Heaviside step function	x_i	=	spatial variable in medium at rest
$H_0^{(2)}$	=	Hankel function	β	=	$\sqrt{1-M^2}$
i	=	the imaginary unit	$\delta(\cdot)$	=	Dirac delta function
k	=	wave number	δ_{ij}	=	Kronecker delta
M	=	Mach number	η_i	=	$x_i + U_i t$
$\hat{n}_i$	=	components of surface normal $\hat{\boldsymbol{n}}$	ρ	=	local fluid density
P_{ij}	=	compressive stress tensor	ρ'	=	unsteady fluid density
p	=	unsteady fluid pressure	ω	=	$2\pi f$, circular frequency
p'	=	sound pressure radiated to observer	ξ_i	=	Prandtl-Glauert transformation variable
T_{ij}	=	Lighthill stress tensor	$()_0$	=	subscript denotes ambient state of variable

* Research Scientist, Computational Modeling and Simulation Branch, Mail Stop 128, Senior Member AIAA.
† Senior Research Scientist, Computational Modeling and Simulation Branch, Mail Stop 128, Senior Member AIAA.
‡ Senior Research Scientist, Computational Modeling and Simulation Branch, Mail Stop 128, Associate Fellow AIAA.
§ Senior Research Scientist, Computational Modeling and Simulation Branch, Mail Stop 128.

I. Introduction

HYBRID methods have been in use for several years to predict airframe noise from the components of multi-element high-lift wings [1 – 7] and undercarriages [8 – 10]. These hybrid methods involve a finely resolved computational fluid dynamics (CFD) simulation of the near field flow that is used as input to an acoustic formulation that predicts noise radiated to a given observer. The acoustic formulations discussed herein are those based on Lighthill's acoustic analogy [11], in particular, the Ffowcs Williams and Hawkings (FW-H) equation [12].

The FW-H equation, the most general form of the acoustic analogy, exactly formulates aerodynamic noise generated by a solid surface in arbitrary motion. The formulation describes this noise in terms of three source distributions. Two of these source terms are distributed on a surface, and are referred to in the literature as the "monopole term" and "dipole term." Both monopole and dipole contributions to the total noise can be determined by the integration of these terms on a solid surface. The third source, or "quadrupole term," is a volume distribution, and its inclusion in a noise prediction can be accounted for in two ways: by integration of the quadrupole term itself throughout a sufficiently large volume surrounding the solid surface, or by integration of the monopole and dipole terms on a permeable surface that encloses such a volume. Throughout this paper, the terminology "volumetric source" will be used to refer to any flow phenomena that give rise to a non-zero value for the volume (quadrupole) integral in the solution of the FW-H equation.

In the use of acoustic-analogy based methods to predict noise from high-lift wing configurations, the FW-H equation is most typically applied without its quadrupole term. The omission of this term is based on the assumption that the contribution to the total noise of volumetric sources outside a chosen integration surface is negligible. Therefore, the choice itself of that integration surface becomes of critical importance. Recent authors have published significant differences in radiated noise from high-lift wing configurations, depending on the location of the integration surface. For instance, Singer, et al. [4] published results in which differences in amplitude and directivity were most pronounced between predictions for which the FW-H integration surface was coincident with the solid surface of the wing and those evaluated by integration on an off-body, permeable surface.

Current high-lift noise predictions are no exception, as will be demonstrated in Section III-B. Important issues are raised by the observation that significant differences in radiated noise can result from the choice to integrate the FW-H equation on a solid or permeable surface. If volume sources are truly negligible for high-lift noise prediction, then there is an internal inconsistency in the flow calculations that are currently used as input to the noise prediction process. However, if volume sources are important for airframe noise prediction, then they must be appropriately incorporated into the development of future prediction tools.

In the following section, the acoustic formulation is described. The FW-H equation and its integral solutions are presented in a manner that applies to an impermeable surface that coincides with the solid body as well as porous, off-body surfaces. Because the flow calculations used as input for this work are solutions of the two-dimensional Navier-Stokes equations, the acoustic predictions are facilitated with a two-dimensional formulation of the FW-H equation [13].

In Section III-A, as a test case, a vortex in uniform flow is acoustically analyzed in regard to its movement through a FW-H integration surface. Both surface and volume integrals are calculated and compared with respect to their contributions to the radiated sound. An airframe noise prediction is then studied in detail in Section III-B. A flow calculation for a high-lift wing configuration is used as input for surface and volume integration of the FW-H equation. The volumetric source contribution to the total noise is accounted for in two ways: by direct evaluation of the quadrupole source term of the FW-H equation within a suitable volume, and by integration on a permeable surface that encloses that volume. The internal consistency of the CFD solution is then assessed by comparison of the radiated noise that is predicted by the permeable surface integration and by the sum of the integrals on the solid surface and within the volume.

II. Acoustic Formulation

The acoustic formulation used herein is a two-dimensional implementation of the FW-H equation in the frequency domain [13]. The differential equations that govern the propagation of sound radiated from a surface in arbitrary motion, as originally proposed by Ffowcs Williams and Hawkings [12], are briefly reviewed. With the assumption of uniform, rectilinear motion, the integral solutions of these equations are then described in a two-dimensional formulation in the spectral domain. In the spectral domain, an exact formulation is available that avoids the "tail effect" associated with the two-dimensional solution in the time domain.

A. The Ffowcs Williams and Hawkings Equation

Ffowcs Williams and Hawkings [12] extended the work of Lighthill [11] and Curle [14] to the formulation of aerodynamic sound generated by a surface in arbitrary motion. In a manner similar to that of Lighthill, they recast the equations of fluid motion in the form of an inhomogeneous wave equation. A critical aspect in the development of the FW-H equation was the casting of certain flow variables as generalized functions. Although their result in [12] was formally presented for an impenetrable surface, Ffowcs Williams and Hawkings clearly understood that the mathematical surface in their formulation did not have to be coincident with the solid body. Formulations for permeable surfaces were published afterward, e.g., Dowling and Ffowcs Williams [15], Crighton, et al. [16] and Brentner and Farassat [17]. Because both solid and porous surfaces are considered in the present work, a unified presentation that closely follows that of Brentner and Farassat [17] is given below.

Consider a closed, non-deformable surface defined by $f(\vec{\boldsymbol{x}},t)=0$, moving along a velocity vector $\vec{\boldsymbol{v}}$ with Cartesian components v_i. The function f is defined such that $f<0$ in the volume interior to the surface, and $f>0$ in the volume exterior to the surface. Let $\hat{\boldsymbol{n}}=\vec{\nabla}f$ denote the unit vector, with Cartesian components $\hat{n}_i$, that is normal to the surface and directed outward into the fluid. The fluid variables ρ and u_i are local measures of the density and velocity, respectively. The analogous quantities in the medium at rest are denoted by the subscript "0," while perturbation quantities are denoted with a "prime" ($'$) superscript. Ffowcs Williams and Hawkings developed their formulation by describing certain flow variables as generalized functions. Such a function assumes its quiescent value interior to the surface, and retains its local value outside the surface (see [11, 17]).

The FW-H equation can be written

$$\left[\frac{\partial^2}{\partial t^2}-c_0^2\frac{\partial^2}{\partial x_i\partial x_i}\right]\left[H(f)\rho'\right]=\frac{\partial^2}{\partial x_i\partial x_j}\left[H(f)T_{ij}\right]-\frac{\partial}{\partial x_i}\left[L_i\delta(f)\right]+\frac{\partial}{\partial t}\left[B\delta(f)\right] \tag{1}$$

where c_0 is the ambient sound speed, and

$$T_{ij}=\rho u_i u_j+P_{ij}-c_0^2\rho'\delta_{ij}\,,\qquad L_i=P_{ij}\hat{n}_j+\rho u_i(u_n-v_n)\,,\qquad B=\rho_0 v_n+\rho(u_n-v_n) \tag{2}$$

The Lighthill stress tensor T_{ij} contributes to the quadrupole term on the right-hand side of Eq. (1), while L_i and B contribute, respectively, to the dipole and monopole terms. $H(f)$ and $\delta(\cdot)$ respectively denote the Heaviside step function and the Dirac delta function. The inviscid compressive stress tensor $P_{ij}=p\delta_{ij}$ is used in this work, where p denotes the unsteady part of the pressure, and δ_{ij} is the Kronecker delta. The quantities u_n and v_n are, respectively, the components of the fluid and surface velocities that are normal to the surface $f=0$, i.e., $u_n=u_i\hat{n}_i$ and $v_n=v_i\hat{n}_i$. Throughout the paper, unless otherwise noted, the summation convention applies to repeated indices. It is re-emphasized here that Eqs. (1) and (2) are valid whether the surface is on or off the solid body. When the surface f is coincident with the solid body, the expressions for L_i and B are simplified by setting $u_n=v_n$ in Eq. (2).

Denote by $\vec{\boldsymbol{x}}=[x_1,x_2,x_3]^T$ the position of an observer exterior to the surface $f=0$. For an observer located in the far field, the acoustic pressure is $p'(\vec{\boldsymbol{x}},t)=c_0^2\rho'(\vec{\boldsymbol{x}},t)$, and the solution of the FW-H equation can be written in the form

$$p'(\vec{\boldsymbol{x}},t)=p'_T(\vec{\boldsymbol{x}},t)+p'_L(\vec{\boldsymbol{x}},t)+p'_Q(\vec{\boldsymbol{x}},t) \tag{3}$$

The three terms on the right-hand side of Eq. (3) represent, from left to right, the radiated sound due to the monopole (or thickness term), dipole (or loading term), and quadrupole source terms in Eqs. (1) and (2). Integral representations for these three terms are dependent upon the particular choice of derivation. Time domain solutions for p'_T and p'_L that are amenable to numerical implementation have been derived by Farassat and Succi [18]. A useful formulation for the volume integral p'_Q is derived by Farassat and Brentner [19].

B. Two Dimensional Formulation

In [13], Lockard derives a frequency-domain formulation for the FW-H equation in two spatial dimensions. Eq. (1) is restricted to the Cartesian coordinate indices *i* = 1, 2, and solved with the appropriate two-dimensional Green's function. The resulting solution is then restricted to uniform rectilinear motion, i.e., $f = f(\vec{x} + \vec{U}t)$, where $\vec{U}$ is a velocity vector with constant components U_i. In this case, the two-dimensional FW-H equation is

$$\left[\frac{\partial^2}{\partial t^2} + U_i U_j \frac{\partial^2}{\partial \eta_i \partial \eta_j} + 2U_i \frac{\partial^2}{\partial \eta_i \partial t} - c_0^2 \frac{\partial^2}{\partial \eta_i \partial \eta_j}\right]\left[H(f)\rho'\right] = \frac{\partial^2}{\partial \eta_i \partial \eta_j}\left[H(f)T_{ij}\right] - \frac{\partial}{\partial \eta_i}\left[L_i \delta(f)\right] + \frac{\partial}{\partial t}\left[B\delta(f)\right] \quad (4)$$

where $\eta_i = x_i + U_i t$ and the derivatives $\partial / \partial \eta_i$ are identical to $\partial / \partial x_i$.

Upon application of the Fourier transform to Eq. (4), the resulting frequency-domain equation is solved with the use of the Green's function

$$G(x, y) = \frac{i}{4\beta} e^{i\left[U_i k (x_i - y_i)/\beta^2\right]} H_0^{(2)}\left(\frac{k}{\beta^2}\sqrt{x_i^2 + \beta^2 y_i^2}\right) \quad (5)$$

The spatial coordinates x_i and y_i are, respectively, the locations of the observer and the source point on the surface $f(\vec{x}, t)$. The symbol β is the Prandtl-Glauert factor $\sqrt{1 - M^2}$, *k* is the wave number, *i* is the imaginary unit, and $H_0^{(2)}$ is the Hankel function of the second kind, of order zero. In the frequency domain, the sound radiated to the far field can be written

$$p'(\vec{\eta}, \omega) = p'_T(\vec{\eta}, \omega) + p'_L(\vec{\eta}, \omega) + p'_Q(\vec{\eta}, \omega) \quad (6)$$

where the thickness and loading noise terms are given by

$$p'_T(\vec{\eta}, \omega) = -\int_{f=0} i\omega B(\vec{\xi}, \omega) G(\vec{\eta}; \vec{\xi})\, d\ell \;, \qquad p'_L(\vec{\eta}, \omega) = -\int_{f=0} L_i(\vec{\xi}, \omega) \frac{\partial G(\vec{\eta}; \vec{\xi})}{\partial \xi_i}\, d\ell \quad (7)$$

The variable $\vec{\xi}$ in the Green's function is associated with a Prandtl-Glauert transformation (See [13] for details). The noise due to volumetric sources is given by the integral

$$p'_Q(\vec{\eta}, \omega) = -\int_{f>0} T_{ij}(\vec{\xi}, \omega) \frac{\partial^2 G(\vec{\eta}; \vec{\xi})}{\partial \xi_i \partial \xi_j}\, d\vec{\xi} \quad (8)$$

The source terms in Eqs. (7) and (8) can be written

$$T_{ij} = \rho(u_i - U_i)(u_j - U_j) + (p - c_0^2 \rho')\delta_{ij} \;, \quad L_i = \left[p\delta_{ij} + \rho(u_i - 2U_i)u_j\right]\hat{n}_j, \quad B = \rho u_n \quad (9)$$

The Green's function derivatives in Eqs. (7) and (8) that are used in this study can be found in [19]. It is restated here that the term "volumetric source" is used to refer to any flow phenomena for which the integral in Eq. (8) is non-zero.

III. Volumetric Source Contributions in Hybrid Method Predictions

The frequency-domain, two-dimensional FW-H formulation discussed in the previous section is applied to two problems. The first, a simple test case involving a vortex convecting in a uniform flow, yields useful information in regard to volumetric sources passing through a porous integration surface. The second, a three-element high-lift airfoil configuration, is acoustically analyzed with the following purposes in mind: to determine the relative contribution of volumetric sources and thereby the internal consistency of the flow calculation, and to highlight the crucial importance of choosing an appropriate integration surface. Note that all enumerated quantities in this study are expressed in a dimensionless fashion, according to the following normalization.

$$f = \frac{\tilde{f} L}{c_0} \;, \qquad t = \frac{\tilde{t}\, c_0}{L} \;, \qquad p = \frac{\tilde{p}}{\rho_0 c_0^2} \quad (10)$$

where $\tilde{f}$, $\tilde{t}$, and $\tilde{p}$ can be expressed in units of measure, and L is a characteristic length scale for the problem under consideration.

A. Test Case: Vortex in Uniform Flow

To test the implementation of the volume integral in Eq. (8), a Taylor vortex [21] is allowed to convect through a FW-H surface. The Taylor vortex is a solution to the Navier-Stokes equations, and would only radiate noise as the vortex decayed. In the current test case, the vortex does not experience any significant decay over the time scale of the problem. However, as the vortex passes through the FW-H surface, the vortex flow field makes a significant contribution to the surface integration terms in Eq. (7). Therefore, the volume integration in Eq. (8) is expected to cancel the contribution from the surface integrals as the vortex passes.

The mean flow Mach number is 0.75 and the peak vortex velocity is 0.15. The pressure field is determined by Bernouilli's equation. The viscosity is chosen such that the vortex velocity is essentially zero at a radius of 5. At $t = 0$, the vortex is at the origin, as shown in the schematic in Fig. 1. A square FW-H surface of length 10 on each side surrounds the vortex at $t = 0$. Each side of the square is discretized with 51 points. (Increasing the resolution to 101 points did not change the results.) As the vortex convects downstream, the radiated sound is calculated in the shaded rectangular region in Fig. 1, given by $\{5 \le x \le 25\} \times \{-5 \le y \le 5\}$. Fig. 2 shows the pressure field of the vortex as it passes the center of the domain. Because the calculation is performed in the frequency domain, a period of 40 is used so that the vortex passes entirely through the FW-H integration region before another vortex is generated.

Fig. 3 shows the directivity for observers at a radius of 100 when only the surface terms are included in the FW-H integration. In general, the error made by such a prediction that does not include the volume integration can vary significantly with the observer's location. Although a crude approximation, one could use the amplitudes in Fig. 3, scaled by the approximate vortex strength, to determine whether the error might be negligible in other problems.

The time history for the sound radiated to an observer at $(x, y) = (0, 100)$ is shown in Fig. 4. This time history is obtained by an FFT post-processing of the spectral output of the FW-H code. The porous surface calculation is compared with the time history from the volume calculation as well as the sum of both calculations. The volume integration does indeed cancel the surface integration during $10 \le t \le 30$, when the vortex is entirely within the "volume" of integration. Fig. 5 shows the imaginary part of the integrand in Eq. (8). Clearly, the positive (red) and negative (blue) contributions would cancel in the interior of the domain. The truncation of the domain of integration at $x = 5$ produces the signal that cancels the contribution from the surface terms. The truncation of the domain at $x = 25$ produces the blip seen at $t > 30$. Nonetheless, the desired cancellation of the signal from the surface terms has been demonstrated. The significance of erroneous noise caused by hydrodynamic phenomena passing through FW-H surfaces will be case dependent. However, an important point has been demonstrated. Because volume integrations are costly, especially in three-dimensional problems, avoiding volume integrations requires that the permeable integration surface be carefully chosen to avoid significant flow features, e.g., wakes, that may exit through the surface.

B. Case Study: High-Lift Configuration

The configuration under present consideration is a three-element high-lift wing profile, whose geometry and pressure field are shown in Fig. 6. This unsteady Reynolds-averaged Navier-Stokes (URANS) calculation, in two spatial dimensions, simulates a Mach 0.2 flow at a mean-chord-based Reynolds number of 10 million. The code CFL3D [22], developed at NASA Langley Research Center, was used for the computations. This CFD calculation employs the SST k-ω turbulence model of Menter [23] with the production term set to zero within the cove region, following the work of Khorrami, et al [7]. The entire flow field contains approximately 1.3 million points, and is highly resolved in those areas that are important to the noise prediction process. For example, a complex shear-layer flow is generated in the slat cove region, as shown in the density perturbation plot in Fig. 7. This region contains approximately 400,000 points. The density field in Fig. 7 shows the irregular acoustic radiation generated by the unsteadiness in the cove region. The circular wavefronts of the propagating sound above the slat are evident, and a complex interference pattern is seen in the vicinity of the cove. Interference as a result of reflections of acoustic waves from the airfoil surface is expected, but these waves may also be influenced by the flow in the cove.

This URANS computation is used as input to the FW-H equation as formulated in Section III-B. The time record for the acoustic predictions contains 2048 samples, spanning a dimensionless time of approximately 1.69.

Every third time step in the CFD simulation is used. Integration of the FW-H equation is performed on solid-body and off-body surfaces, shown in Fig. 8. Note that the off-body surface in Fig. 8 is located near the outer edge of the boundary layer in places where it may visually appear coincident with the body. The vorticity field in Fig. 9 shows that there is a significant wake from the flap that cuts through the dashed portion or the porous surface in Fig. 8. Hence, there is the potential for erroneous noise sources to be generated as vortices in the wake pass through the surface, as demonstrated in the test case of the previous subsection. The unsteadiness in the wake contains dimensionless frequencies below 75. Fig. 10 shows a comparison between directivity patterns for $f < 75$ that result by integrating the FW-H equation on the solid and off-body surfaces in Fig. 8. In addition, a FW-H calculation was performed using the porous surface P1 in Fig. 8 with the dashed portion of surface removed. The observers are located on a circle located 5 chords from the airfoil. Clearly, neglecting the portion of the porous surface around the flap produces better agreement with the solid surface result. Attempts to add the volume contribution to the solid surface prediction were not entirely successful because only part of the wake could be included in the volume integration. However, the difficulties with the flap wake are restricted to very low frequencies. The inclusion of the flap region has almost no effect on the solution for $f > 75$. Therefore, the analysis is restricted to this mid-to-upper frequency range for the remainder of the paper.

Fig. 11 shows two directivity patterns for the acoustic pressure that are predicted for $f > 75$ by integrating the FW-H equation on the two surfaces in Fig. 8. The observers are located on a circle located 5 chords from the airfoil. There is a significant difference in both amplitude and directivity of the major lobes. This difference is consistent with the previous work of other authors, e.g. Singer, et al [4]. The solution of the FW-H equation dictates that the difference between the two predictions in Fig. 11 must be the result of volume sources within the off-body, porous surface. Fig. 12 shows the spectra from the two computations for an observer at 300 degrees, measured as a positive angle from the downstream direction. Most of the discrepancy between the two predictions occurs in the frequency range $250 < f < 450$, as detailed in Fig. 13. In this frequency range, the acoustic wavelength is approximately the same size as the vortices in the cove.

The internal consistency of the flow calculation can be assessed by comparison of the radiated noise that is predicted by the porous surface integral to the sum of the integrals on the solid surface and within the volume. In Fig. 14, the same directivities as in Fig. 11 are plotted, with the addition of the directivity predicted by the sum of the FW-H integral on the solid-body surface combined with the integral over the volume between the solid surface and the porous surface P1 (blue line). The agreement is good between the P1 surface integration (red line) and the sum of the integrals on the solid surface and within the volume (blue line). Although these two predictions are not identical, as the FW-H equation dictates, the difference is small enough to be attributed to numerical error in the input flow simulation. Furthermore, the spectra are in good agreement for all frequencies above 75, including the range $250 < f < 450$, as shown in Fig. 15. Clearly, this level of agreement establishes the internal consistency of the CFD solution, i.e., consistency with the Navier-Stokes equations. Furthermore, this agreement indicates that a high-lift noise prediction that relies solely on surface pressure is inadequate for the frequency range of interest.

IV. Concluding Remarks

The relative importance of volumetric sources to the prediction of airframe noise has been the subject of a preliminary examination. To the authors' knowledge, this work contains the first direct calculation of the volume quadrupole contribution to the far-field noise associated with a high-lift wing configuration. By establishing the internal consistency of the input flow calculation, it is now clear that the contribution of volumetric sources to the total noise is non-negligible in high-lift simulations. Therefore, it is insufficient to predict the far field noise solely by the integration of pressure on the solid surface. In order to appropriately account for these volumetric sources without resorting to the costly direct calculation of the FW-H volume integral, two steps in the acoustic prediction process must be judiciously balanced. First, the spatial extent to which the near-field flow simulation is adequately resolved must be determined. Secondly, the permeable FW-H integration surface must be carefully placed so that there is sufficient resolution to account for propagation of acoustic waves in the frequency range of interest, but without significant hindrance from an exiting wake. As for the manner in which these results impact the development of airframe noise prediction tools, the exact nature of the physical phenomena occurring in the cove region that results in a significant volume contribution must be determined. Further analysis will be required to assess whether simple models that neglect flow propagation effects can produce reasonable results.

Acknowledgments

The authors would like to express their gratitude to Dr. F. Farassat of NASA Langley Research Center and Prof. G. M. Lilley of Pennsylvania State University for their consultation time involved with this research.

References

1. Macaraeg, M. G., "Fundamental Investigations of Airframe Noise," AIAA-1998-2224, 4th AIAA/CEAS Aeroacoustics Conference, 1998.
2. Streett, C. L., "Numerical Simulation of Fluctuations Leading to Noise in a Flap-Edge Flow Field," AIAA-1998-0628, 36th Aerospace Sciences Meeting, 1998.
3. Streett, C. L., "Numerical Simulation of a Flap-Edge Flow Field," AIAA-1998-2226, 4th AIAA/CEAS Aeroacoustics Conference, 1998.
4. Singer, B. A., Lockard, D. P., and Brentner, K. S., "Computational Aeroacoustic Analysis of Slat Trailing Edge Flow," *AIAA Journal*, Vol. 38, No. 9, 2000, pp. 1558 - 1564.
5. Singer, B. A., Brentner, K. S., Lockard, D. P., and Lilley, G. M., "Simulation of Acoustic Scattering from a Trailing Edge," *Journal of Sound and Vibration*, Vol. 230, No. 3, 2000, pp. 541 - 560.
6. Khorrami, M. R., Singer, B. A., and Berkman, M. E., "Time Accurate Simulations and Acoustic Analysis of a Slat Free-Shear Layer," AIAA Paper 2001-2155, 2001.
7. Khorrami, M. R., Singer, B. A., and Lockard, D. P., "Time Accurate Simulations and Acoustic Analysis of a Slat Free-Shear Layer: Part II," AIAA Paper 2002-2579, 2002.
8. Souliez, F. J., Long, L. N., Morris, P. J., "Landing Gear Aerodynamic Noise Prediction Using Unstructured Grids," AIAA-2002-0799, 40th AIAA Aerospace Sciences Meeting, 2002.
9. Lockard, D. P., "A Comparison of Ffowcs Williams – Hawkings Solvers for Airframe Noise Applications," AIAA-2002-2580, 8th AIAA/CEAS Aeroacoustics Conference, 2002.
10. Lockard, D. P., Khorrami, M. R., and Li, F., "Aeroacoustic Analysis of a Simplified Landing Gear," AIAA-2003-3111, 9th AIAA/CEAS Aeroacoustics Conference, 2003.
11. Lighthill, M. J., "On Sound Generated Aerodynamically. I. General Theory," *Proceedings of the Royal Society of London*, A 211, 1952, pp. 564 – 587.
12. Ffowcs Williams, J. E. and Hawkings, D. L., "Sound Generation by Turbulence and Surfaces in Arbitrary Motion," *Philosophical Transactions of the Royal Society*, A264, 1969, pp. 321 – 342.
13. Lockard, D. P., "An Efficient, Two-Dimensional Implementation of the Ffowcs Williams and Hawkings Equation," *Journal of Sound and Vibration*, Vol. 229, No. 4, 2000, pp. 897 – 911.
14. Curle, N., "The influence of Solid Boundaries on Aerodynamic Sound," *Proceedings of the Royal Society of London*, A231, 1955, pp. 505-514.
15. Dowling, A. P. and Ffowcs Williams, J. E., *Sound and Sources of Sound*, Ellis Horword, Chichester, England, UK, 1983, Chapter 9, Section 2.
16. Crighton, D. G., Dowling, A. P., Ffowcs Williams, J. E., Heckl, M. and Leppington, F. G., *Modern Methods in Analytical Acoustics*, Lecture Notes, Springer-Verlag, London, 1992, Chapter, 11, Section 10.
17. Brentner, K. S. and Farassat, F., "Analytical Comparison of the Acoustic Analogy and Kirchoff Formulation for Moving Surfaces," *AIAA Journal*, Vol. 36, No. 8, 1998, pp. 1379 – 1386.
18. Farassat. F. and Succi, G. P., "The Prediction of Helicopter Rotor Discrete Frequency Noise," *Vertica*, Vol. 7, No. 4, 1983, pp. 309-320.
19. Farassat, F. and Brentner, K. S., "The Uses and Abuses of the Acoustic Analogy in Helicopter Rotor Noise Prediction," *Journal of the American Helicopter Society*, Vol. 33, 1988, pp. 29 – 36.
20. Gloerfelt, X., Bailly, C., and Juve, D., "Direct Computation of the Noise Radiated by a Subsonic Cavity Flow and Application of Integral Methods," ," *Journal of Sound and Vibration*, Vol. 266, 2003, pp. 119 – 146.
21. Panton, R. L., *Incompressible Flow*, John Wiley & Sons, New York, 1984, pp. 286 – 7.
22. Rumsey, C. and Biedron, R. and Thomas, J., "CFL3D: Its History and Some Recent Applications," NASA TM 112861, May 1997, presented at the Godonov's Method for Gas Dynamics Symposium, Ann Arbor, MI.
23. Menter, F. R., "Zonal Two-equation k-omega Turbulence Models for Aerodynamic Flows", AIAA-93-2906", 1993.

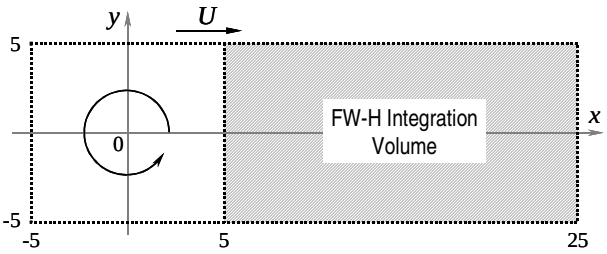

Figure 1. Schematic for vortex in uniform flow.

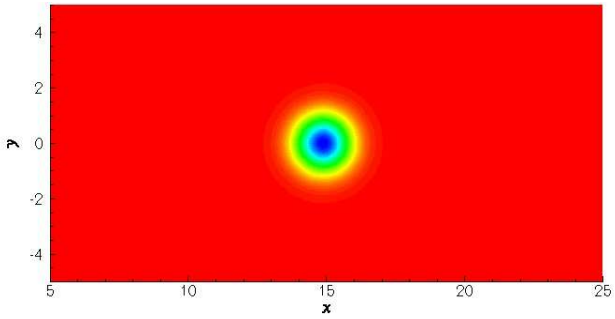

Figure 2. Vortex in uniform flow: pressure field.

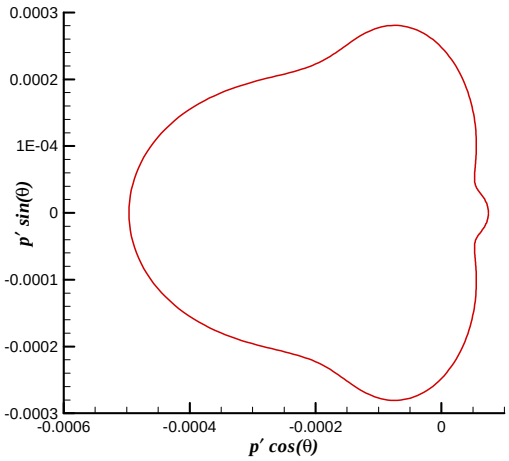

Figure 3. Directivity of noise from FW-H surface integration only.

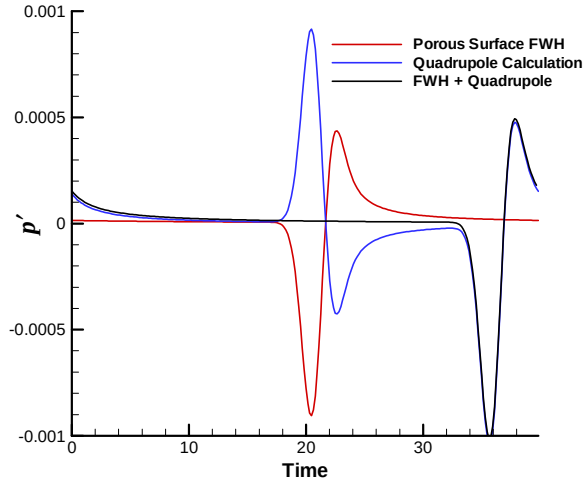

Figure 4. Time history for observer at $(0,100)$.

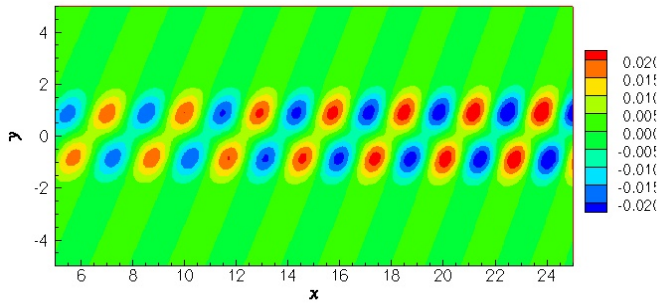

Figure 5. Vortex in uniform flow. Imaginary part of the integrand in Eq. (8).

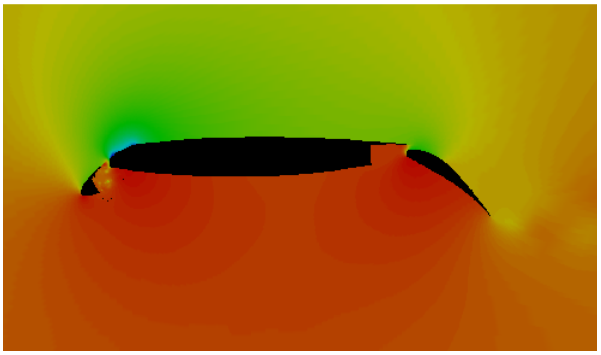

Figure 6. High-lift wing profile: pressure field.

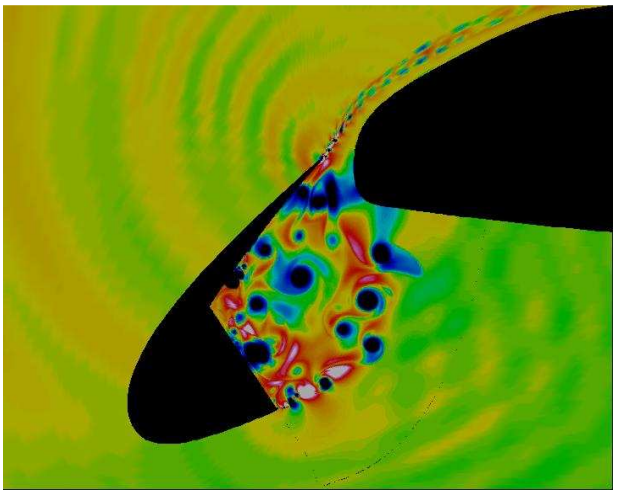

Figure 7. Slat cove region: ρ', perturbation density.

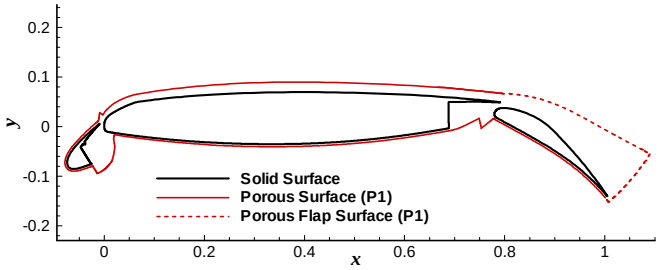

Figure 8. FW-H integration surfaces.

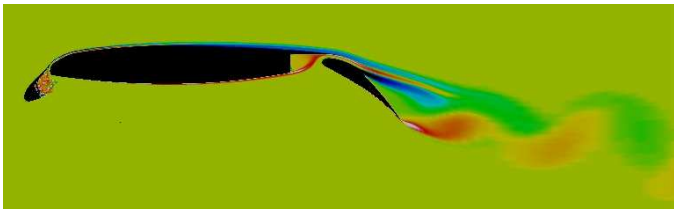

Figure 9. Vorticity field, including flap wake.

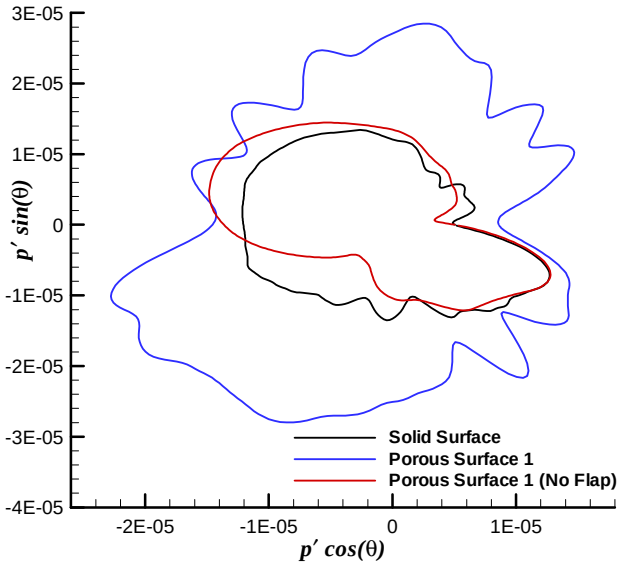

Figure 10. Directivity for $f < 75$ as predicted by integration on surfaces in Fig. 8.

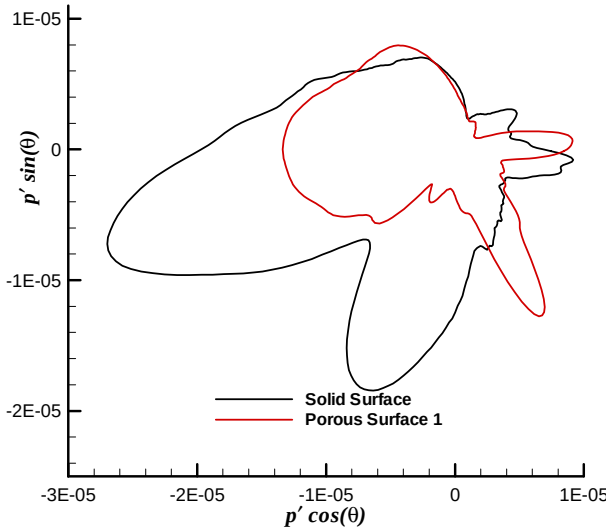

Figure 11. Directivity for $f > 75$ as predicted by integration on surfaces in Fig. 8.

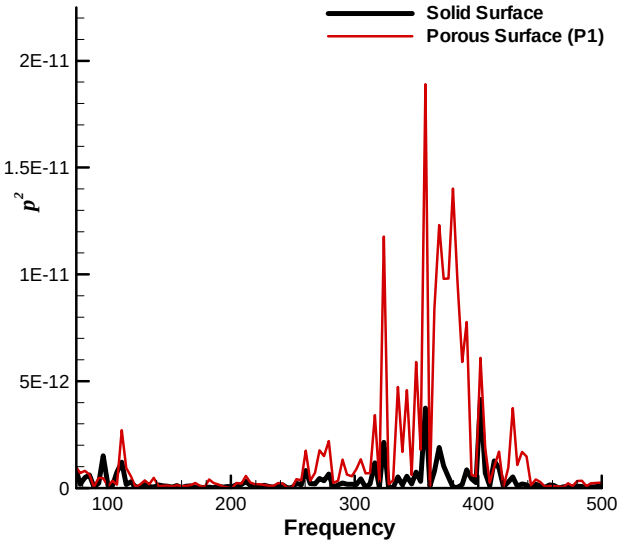

Figure 12. Spectra from predictions in Fig. 11, for one observer at 300 degrees.

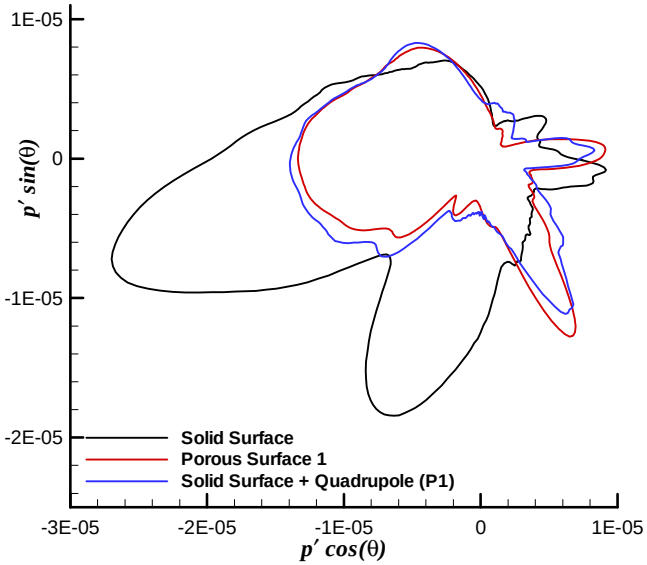

Figure 14. Directivity, same as in Fig. 11 with addition of directivity predicted by summing FW-H integrals on solid surface and within volume.

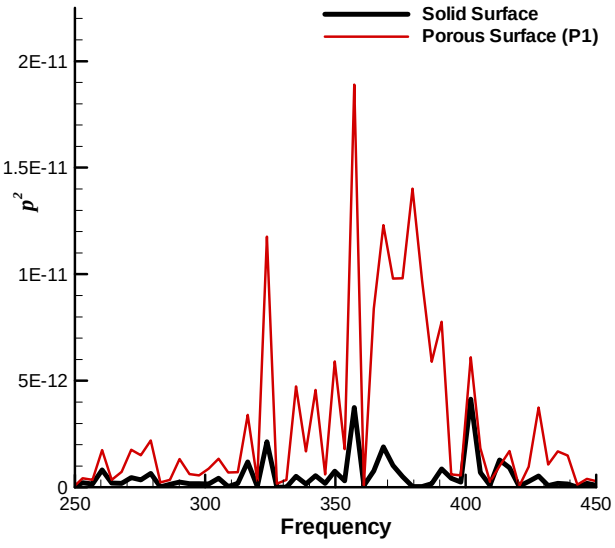

Figure 13. Same plot as in Fig. 12, for the frequency range $250 < f < 450$.

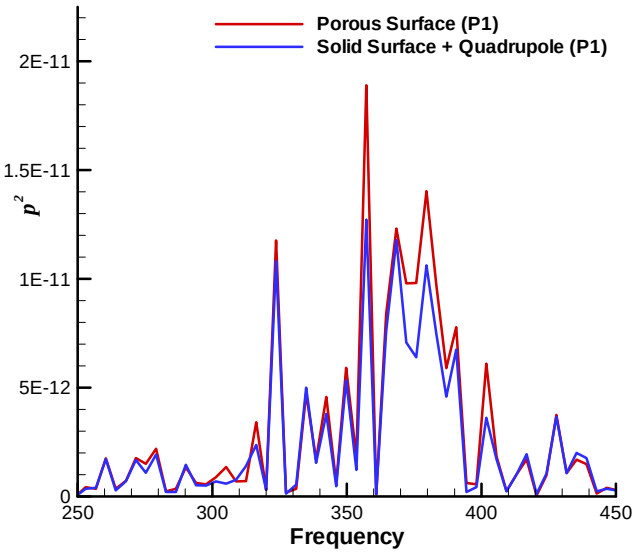

Figure 15. Spectral comparison for two of the predictions in Fig. 14. for $250 < f < 450$. Observer is at 300 degrees.